Supporting Information

High-Performance Ternary Solar Cells by Introducing One Medium Bandgap Acceptor with Complementary Absorption, Reducing Energy Disorder and Enhancing Glass Transition Temperature

Ji Wan,[+] Ivan Dyadishchev,[+] Rui Sun, Qiang Wu, Yao Wu, Meimei Zhang, Svetlana Peregudova, Sergey Ponomarenko, Yuriy Luponosov,[*] Jie Min[*]

J. Wan, R. Sun, Q. Wu, Y. Wu, M. Zhang, Prof. J. Min
The Institute for Advanced Studies, Wuhan University, Wuhan 430072, China
Email: min.jie@whu.edu.cn

Prof. J. Min
Beijng National Laboratory for Molecular Sciences, Beijing 100190, China

I. Dyadishchev, Dr. Peregudova, Prof. S. Ponomarenko, Dr. Yu. Luponosov,
Enikolopov Institute of Synthetic Polymeric Materials Russian Academy of Sciences (ISPM RAS), Moscow 117393, Russia
Email: luponosov@ispm.ru

Dr. Peregudova
Nesmeyanov Institute of Organoelement Compounds of Russian Academy of Sciences, Vavilova St. 28, Moscow, 119991, Russia

[+]J. W. and I. D. contributed equally to this work.

Contents

1. Experimental Section

1.1 Materials

Tetrakis(triphenylphosphine) palladium (0), triphenylphosphine, 1,1-dicyanomethylene-3-indanone and n-butyllithium (2.5 M solutions in hexane) were obtained from Sigma-Aldrich Co. and used without further purification. Tributyl(2-thienyl)stannane, 1,4-dibromo-2,5-dinitrobenzene and 1-bromo-1-hexylheptane were prepared using the procedure described elsewhere. Toluene, dimethyl sulfoxide (DMSO), o-dichlorobenzene (o-DCB), tetrahydrofuran (THF) and pyridine were dried and purified according to the known techniques and then used as solvents. In the case of column chromatography, silica gel 60 (Merck) was taken. All reactions, unless stated otherwise, were carried out under an inert atmosphere using anhydrous solvents. Yao Wu synthesized the Y6 material according to the previous reference.[1] PM6 and PNDIT-F3N were purchased from Solarmer Materials Inc. Solvents (chloroform) were dried and distilled from appropriate drying agents before use. The processes of the purification of solvents are as followed: The purifications involve washing with water several times to remove the ethanol, drying with potassium carbonate, refluxing with calcium chloride, and then distilling.

1.2 General characterization

^{1}H NMR spectra were recorded at a "Bruker WP-250 SY "spectrometer, working at a frequency of 250.13 MHz and utilizing CDCl$_3$ signal (7.25 ppm) as the internal standard. ^{13}C NMR spectra were recorded using a "Bruker Avance II 300" spectrometer at 75 MHz. In the case of ^{1}H NMR spectroscopy, the compounds to be analyzed were taken in the form of 1% solutions in CDCl$_3$. In the case of ^{13}C NMR spectroscopy, the compounds to be analyzed were taken in the form of 5% solutions in CDCl$_3$. The spectra were then processed using the ACD Labs software.

Elemental analysis of C, N and H elements was carried out using a CHN automatic analyzer (CE 1106). Mass-spectra (MALDI) was registered on the Autoflex II Bruker (resolution FWHM 18000), equipped with a nitrogen laser (work wavelength 337 nm) and time-of-flight mass-detector working in reflections mode. The accelerating voltage was 20 kV. Samples were applied to a polished stainless steel substrate. Spectrum was recorded in the positive ion mode. The resulting spectrum was the sum of 300 spectra obtained at different points of the sample. 2,5-Dihydroxybenzoic acid (DHB) (Acros, 99%) and α-cyano-4-hydroxycinnamic acid (HCCA) (Acros, 99%) were used as matrices.

Thermogravimetric analysis was carried out in a dynamic mode within the temperature range of 30-700 °C using an "STA JUPITER 443 F3 NETZSCH" system (Germany). The heating/cooling rate was chosen to be 10 °C/min.

CV measurements were done in 1,2-dichlorobenzene/acetonitrile (4:1) mixture of solvents in a standard three-electrode cell equipped with a glassy carbon working electrode (s = 2 mm^2), platinum plate as the counter electrode, and SCE (saturated calomel electrode) as the reference electrode. The highest occupied molecular orbital (HOMO) and the lowest unoccupied molecular orbital (LUMO) energies were evaluated using the first standard oxidation (φ_{ox}) and reduction (φ_{red}) potentials obtained from CV experiments as E(HOMO) = $-e(\varphi_{ox}+4.40)$ (eV) and E(LUMO) = $-e(\varphi_{red}+4.40)$ (eV), where e is the elementary charge.[2,3]

Absorption profiles were recorded with an absorption spectrometer (Shimadzu UV 2501 PC) at room temperature in diluted chloroform solutions (10^{-5} M) and films cast from chloroform solutions with a concentration of 10 g/L on glass substrates.

1.3 Synthetic procedures

2,2'-(2,5-dinitro-1,4-phenylene)dithiophene (1)

Tributyl(2-thienyl)stannane (5.49 g, 14.7 mmol), 1,4-dibromo-2,5-dinitrobenzene (2.00 g, 6.1 mmol) and Pd(PPh$_3$)$_4$ (0.17 g, 0.15 mmol) were dissolved in 35 mL of dry toluene

and stirred at reflux for 6 hours under argon atmosphere. After completeness of the reaction, the reaction mixture was concentrated under reduced pressure. The crude product was chromatographically purified on a silica gel column eluting with dichloromethane/petroleum ether (1/3, *v/v*) to afford **1** as a yellow solid (1.72 g, 84 % yield). ^{1}H NMR (250 MHz, CDCl$_3$) δ 7.87 (s, 2H), 7.51 (dd, J_1 = 4.88 Hz, J_2 = 1.22 Hz, 2H), 7.19 (dd, J_1 = 3.66 Hz, J_2 = 1.22 Hz, 2H), 7.12 (dd, J_1 = 4.88 Hz, J_2 = 3.66 Hz, 2H). ^{13}C NMR (101 MHz, CDCl$_3$) δ 126.99, 128.37, 128.46, 128.56, 128.89, 134.05. Calcd (%) for C$_{14}$H$_8$N$_2$O$_4$S$_2$: C, 50.59; H, 2.43; N, 8.43; S, 19.29. Found: C, 50.74; H, 2.52; N, 8.39; S, 19.18. HR-MS (MALDI-TOF) *m/z* calcd. for (C$_{14}$H$_8$N$_2$O$_4$S$_2$): 331.99. Found: 331.98.

4,9-bis(1-hexylheptyl)-4,9-dihydrothieno[3,2-b]thieno[2',3':4,5]pyrrolo[2,3-f]indole

Compound **1** (1.30 g, 3.9 mmol) and triphenylphosphine (10.26 g, 39.1 mmol) were dissolved in the 30 mL of *o*-DCB. The reaction was stirred at 180 °C for 12 hours. Then the solvent was removed under a reduced pressure to give the crude compound **2**, which was used as received in the next step without any purification. Then 1-bromo-1-hexylheptane (4.12 g, 15.6 mmol), potassium hydroxide (3.28 g, 58.7 mmol), potassium iodide (0.32 g, 2.0 mmol), and DMSO (25 mL) were added and the mixture was deoxygenated with argon. The resulting solution was stirred at 80 °C until the reaction was complete by TLC. The residue was extracted with ethyl acetate and H$_2$O. The organic layers were combined and dried over Na$_2$SO$_4$, filtered and purified with column chromatography on silica gel using dichloromethane/petroleum ether (1/10, *v/v*) as the eluent to give a pale yellow solid **3** (1.58 g, 65% yield). ^{1}H NMR (250 MHz, CDCl$_3$) δ 7.69 (s, 2H), 7.29 (d, 2H), 7.21 (d, 2H), 4.11 (m, M = 5, J = 6.41 Hz, 2H), 1.63 – 1.78 (m, 8H), 1.16 – 1.32 (overlapping peaks, 32H), 0.78 –0.86 (m, 12H). ^{13}C NMR (101 MHz, CDCl$_3$) δ 14.02, 22.57, 24.11, 29.70, 31.59, 58.47, 108.97, 121.69, 123.61, 135.54, 140.68, 149.69, 151.96. Calcd (%) for C$_{40}$H$_{60}$N$_2$S$_2$: C, 75.89; H, 9.55; N, 4.43; S, 10.13. Found: C, 75.96; H, 9.62; N, 4.38; S, 10.08. HR-MS (MALDI-TOF) *m/z* calcd.

for ($C_{40}H_{60}N_2S_2$): 632.42. Found: 632.40.

4,9-bis(1-hexylheptyl)-4,9-dihydrothieno[3,2-b]thieno[2',3':4,5]pyrrolo[2,3 f]indole-2,7-dicarbaldehyde (4)

n-BuLi (1.40 mL, 2.5 M in hexane) was added dropwise to a solution of compound **3** (1.00 g, 1.6 mmol) in THF (30 mL) at -78 °C under argon. After stirring at the same temperature for 1.5 hours, dry DMF (0.40 mL, 5.2 mmol) was added at once. Then the solution was warmed to room temperature and stirred for several hours. The reaction mixture was poured into water and then extracted with diethyl ether. The combined organic layer was washed with water and brine, dried over Na₂SO4, and evaporated under reduced pressure. The crude product was purified with column chromatography on silica gel using dichloromethane/petroleum ether (1/2, *v/v*) as the eluent to give an orange solid **4** (0.87 g, 80% yield). ¹H NMR (250 MHz, CDCl₃) δ 9.81 (s, 2H), 7.91 (s, 2H), 7.76 (s, 2H), 4.11 (m, M = 5, *J* = 6.41 Hz, 2H), 1.63 – 1.78 (m, 8H), 1.16 – 1.32 (overlapping peaks, 32H), 0.78 – 0.86 (m, 12H). ¹³C NMR (101 MHz, CDCl₃) δ 13.96, 22.49, 24.19, 29.51, 31.49, 38.92, 58.84, 115.71, 129.90, 136.45, 145.55, 151.05, 152.71, 153.15, 184.05. Calcd (%) for $C_{42}H_{60}N_2O_2S_2$: C, 73.21; H, 8.78; N, 4.07; S, 9.31. Found: C, 73.33; H, 8.72; N, 4.01; S, 9.22. HR-MS (MALDI-TOF) *m/z* calcd. for ($C_{40}H_{60}N_2S_2$): 673.38. Found: 673.39.

2,2'-([4,9-bis(1-hexylheptyl)-4,9-dihydrothieno[3,2-b]thieno[2',3':4,5]pyrrolo[2,3-f]indole-2,7-diyl]bis{(Z)methylylidene[(2Z)-3-oxo-1H-indene-2,1 diylidene]})dimalononitrile (TPIIC)

Aldehyde **4** (0.30 g, 0.4 mmol) and 1,1-dicyanomethylene-3-indanone (0.21g, 1.1 mmol) were dissolved in chloroform (10 mL) in a round bottom flask under argon. Then pyridine (2 mL) was added, and the mixture was stirred at 60 °C for 12 h. After cooling to room temperature, the mixture was poured into methanol and filtered. The residue was purified via column chromatography on silica gel using chloroform/petroleum ether (1/1, *v/v*) as the eluent to give a dark green solid **5** (0.25 g, 55% yield). ¹H NMR

(250 MHz, CDCl$_3$) δ 8.91 (s, 2H), 8.67 – 8.76 (m, 2H), 7.91 – 7.97 (m, 2H), 7.68 – 7.81 (overlapping peaks, 6H), 7.47 (s, 2H), 4.11 (m, M = 5, J = 6.41 Hz, 2H), 1.63 – 1.78 (m, 8H), 1.16 – 1.32 (overlapping peaks, 32H), 0.78 – 0.86 (m, 12H). ^{13}C NMR (101 MHz, CDCl$_3$) δ 13.96, 22.50, 24.30, 29.50, 31.47, 36.86, 59.18, 68.85, 114.70, 114.78, 116.39, 121.13, 123.70, 125.26, 134.43, 135.09, 136.13, 137.89, 138.88, 139.89, 141.08, 151.28, 153.53, 154.91, 160.63, 188.32. Calcd (%) for C$_{66}$H$_{68}$N$_6$O$_2$S$_2$: C, 76.12; H, 6.58; N, 8.07; S, 6.16. Found: C, 76.20; H, 6.65; N, 8.05; S, 6.10. HR-MS (MALDI-TOF) *m/z* calcd. for (C$_{40}$H$_{60}$N$_2$S$_2$): 1040.48. Found: 1040.49.
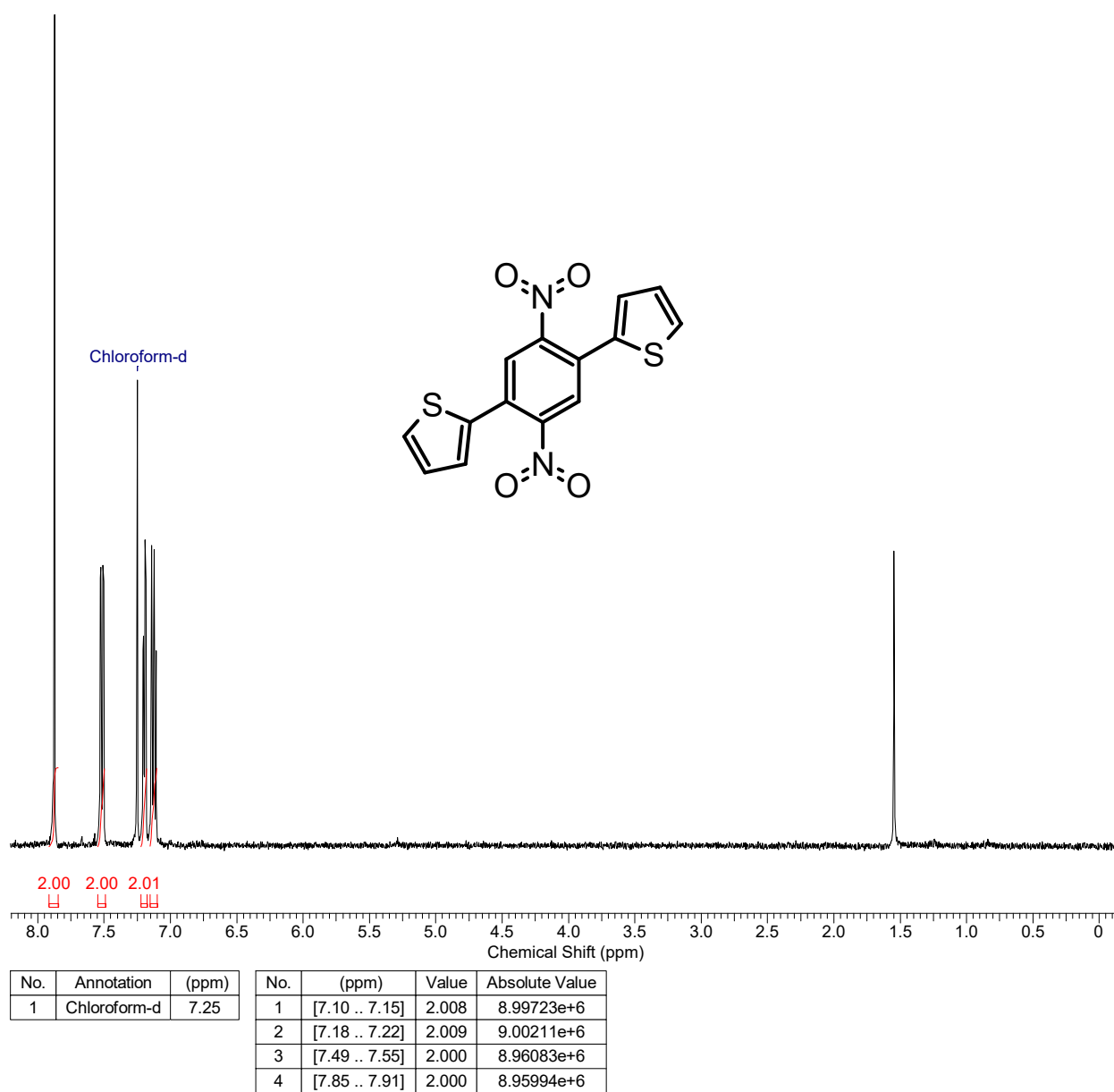
1.4 NMR Spectra

No.	Annotation	(ppm)
1	Chloroform-d	7.25

No.	(ppm)	Value	Absolute Value
1	[7.10 .. 7.15]	2.008	8.99723e+6
2	[7.18 .. 7.22]	2.009	9.00211e+6
3	[7.49 .. 7.55]	2.000	8.96083e+6
4	[7.85 .. 7.91]	2.000	8.95994e+6

Fig. S1 ^{1}H NMR spectrum of compound **1** in CDCl$_3$.

No.	(ppm)	(Hz)	Height
1	126.99	9585.1	0.2025
2	128.37	9689.1	0.2154
3	128.46	9695.7	0.2520
4	128.56	9703.5	0.1169
5	128.89	9728.3	0.2236
6	134.05	10118.1	0.0991

No.	Annotation	(ppm)
1	Chloroform-d	77.00
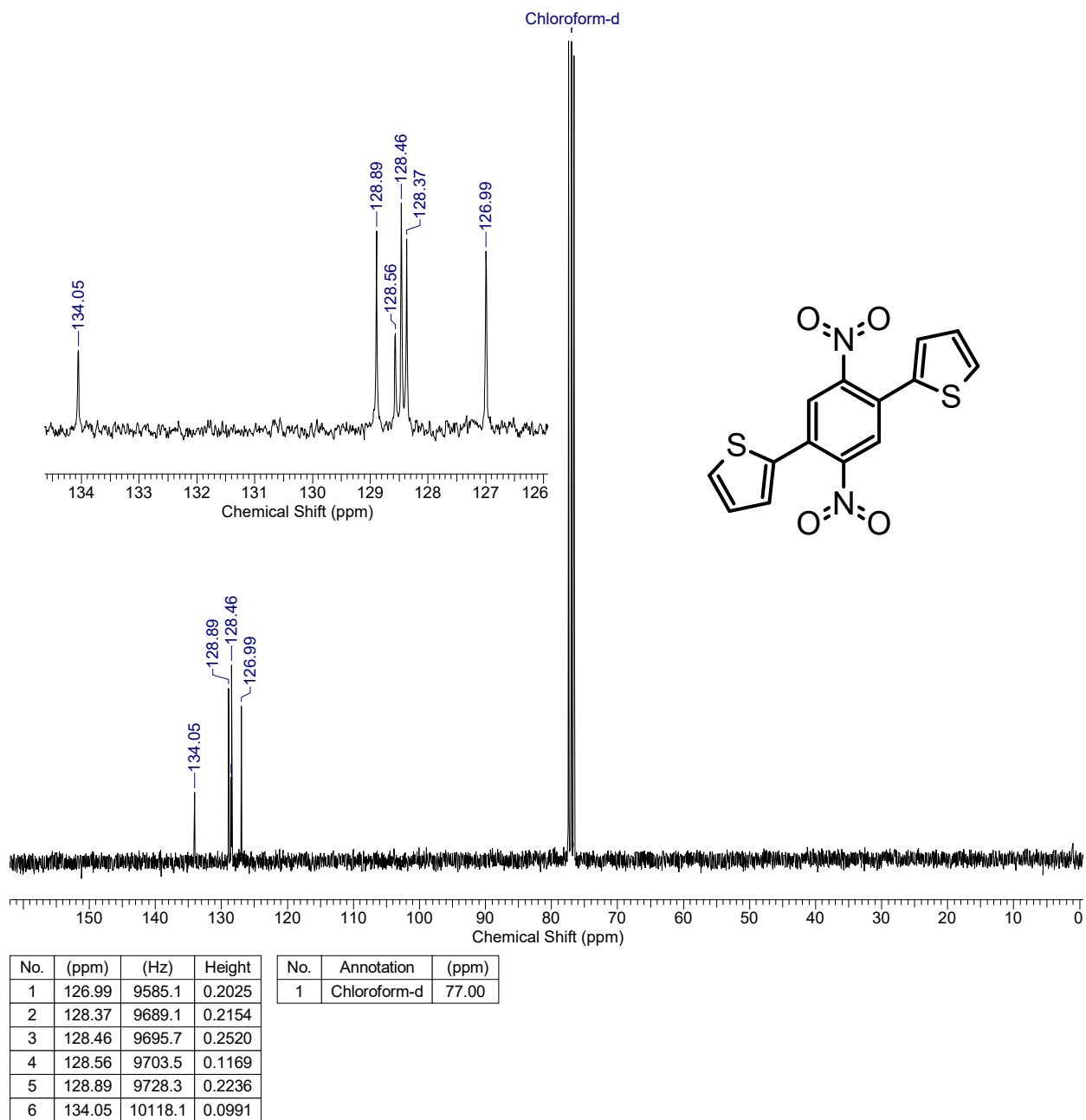
Fig. S2 ^{13}C NMR spectrum of compound **1** in CDCl$_3$.
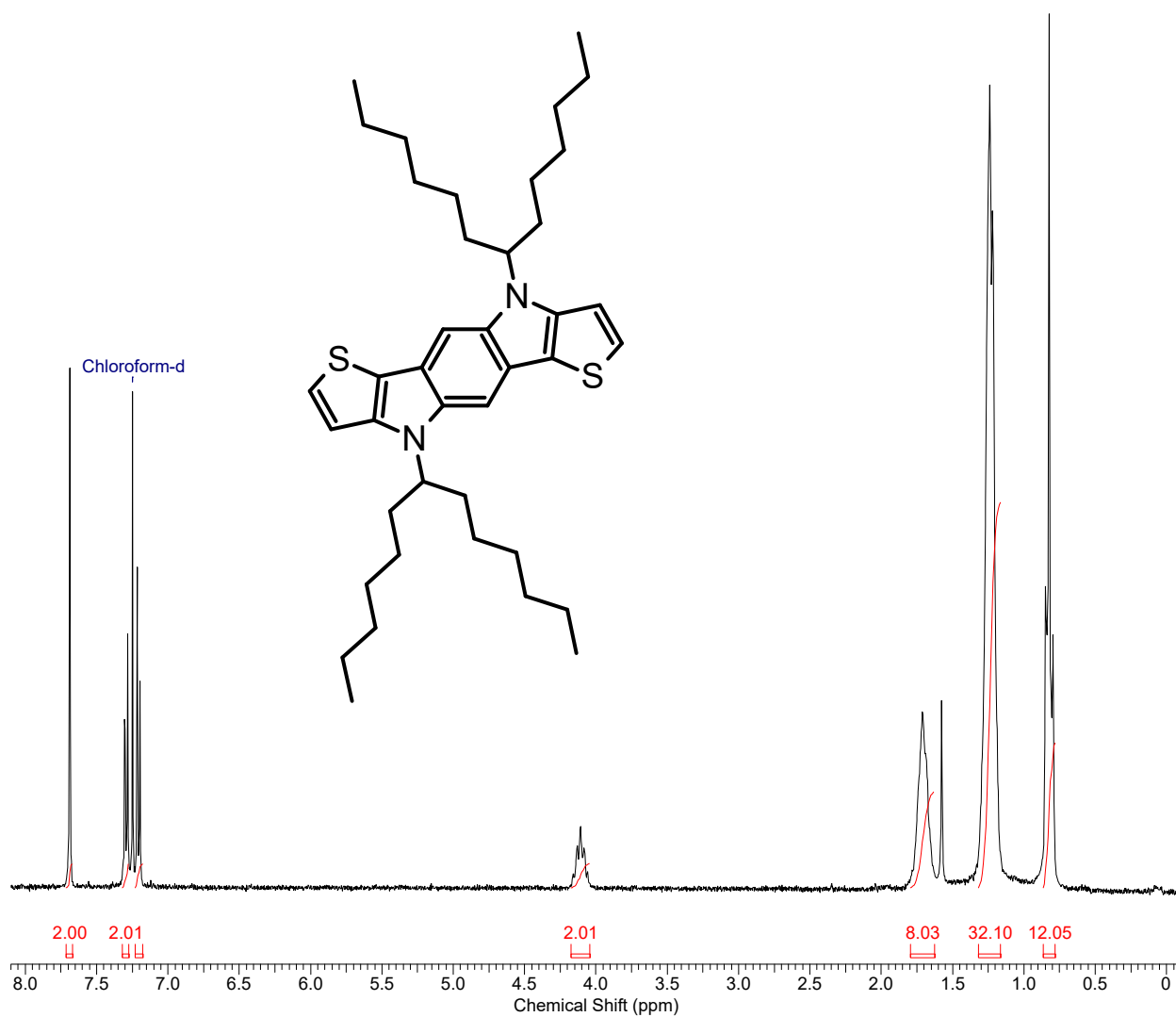
No.	Annotation	(ppm)
1	Chloroform-d	7.25

No.	(ppm)	Value	Absolute Value
1	[0.78 .. 0.87]	12.049	5.26735e+7
2	[1.16 .. 1.32]	32.095	1.40314e+8
3	[1.63 .. 1.80]	8.030	3.51066e+7
4	[4.04 .. 4.18]	2.009	8.78290e+6
5	[7.18 .. 7.23]	1.999	8.73841e+6
6	[7.28 .. 7.32]	2.012	8.79706e+6
7	[7.67 .. 7.71]	2.000	8.74351e+6

Fig. S3 ^{1}H NMR spectrum of compound **3** in CDCl$_3$.

Fig. S4 ¹³C NMR spectrum of compound **3** in CDCl₃.
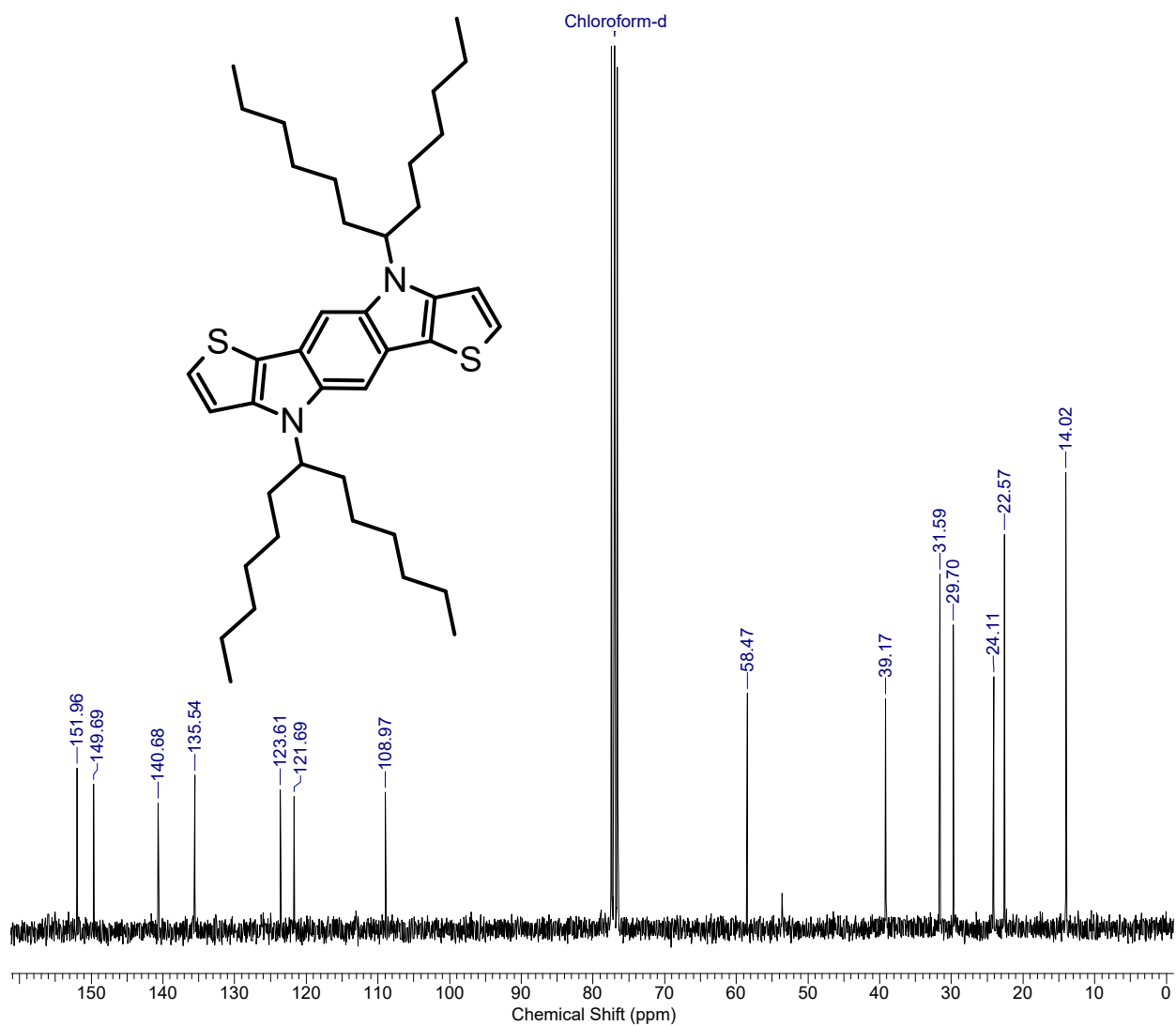
No.	(ppm)	(Hz)	Height
1	14.02	1058.2	0.5255
2	22.57	1703.4	0.4564
3	24.11	1819.5	0.2975
4	29.70	2241.3	0.3552
5	31.59	2384.0	0.4123
6	39.17	2956.8	0.2736
7	58.47	4413.0	0.2796
8	108.97	8224.5	0.1692
9	121.69	9184.9	0.1643
10	123.61	9329.7	0.1722
11	135.54	10230.3	0.1882
12	140.68	10617.9	0.1571
13	149.69	11297.9	0.1782
14	151.96	11469.9	0.1962

No.	Annotation	(ppm)
1	Chloroform-d	77.00
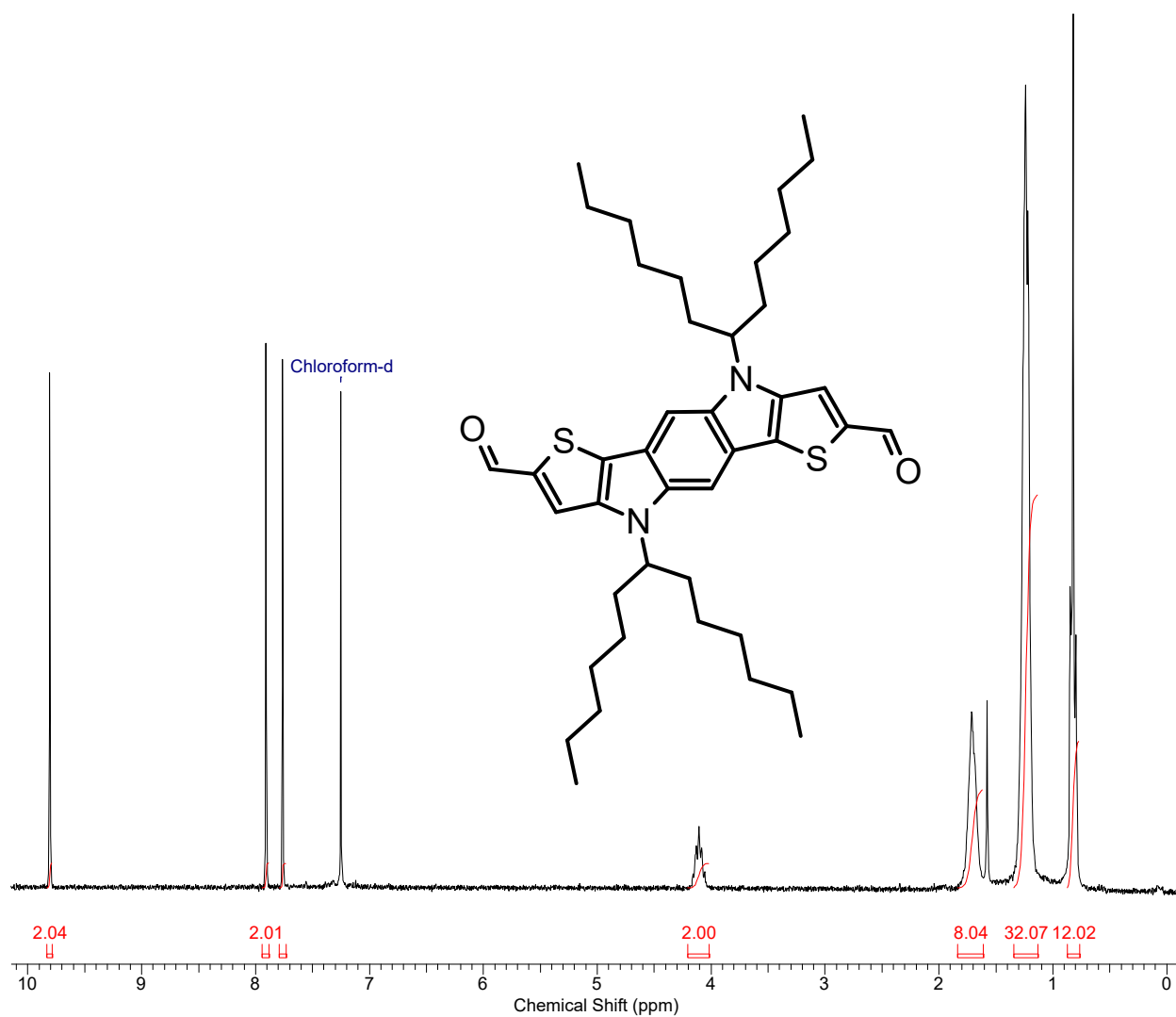
No.	Annotation	(ppm)
1	Chloroform-d	7.25

No.	(ppm)	Value	Absolute Value
1	[0.76 .. 0.87]	12.024	5.37755e+7
2	[1.13 .. 1.34]	32.069	1.43426e+8
3	[1.61 .. 1.84]	8.041	3.59637e+7
4	[4.02 .. 4.21]	2.000	8.94493e+6
5	[7.73 .. 7.79]	2.004	8.96167e+6
6	[7.88 .. 7.94]	2.015	9.01187e+6
7	[9.78 .. 9.83]	2.042	9.13348e+6

Fig. S5 ^{1}H NMR spectrum of compound **4** in CDCl$_3$.
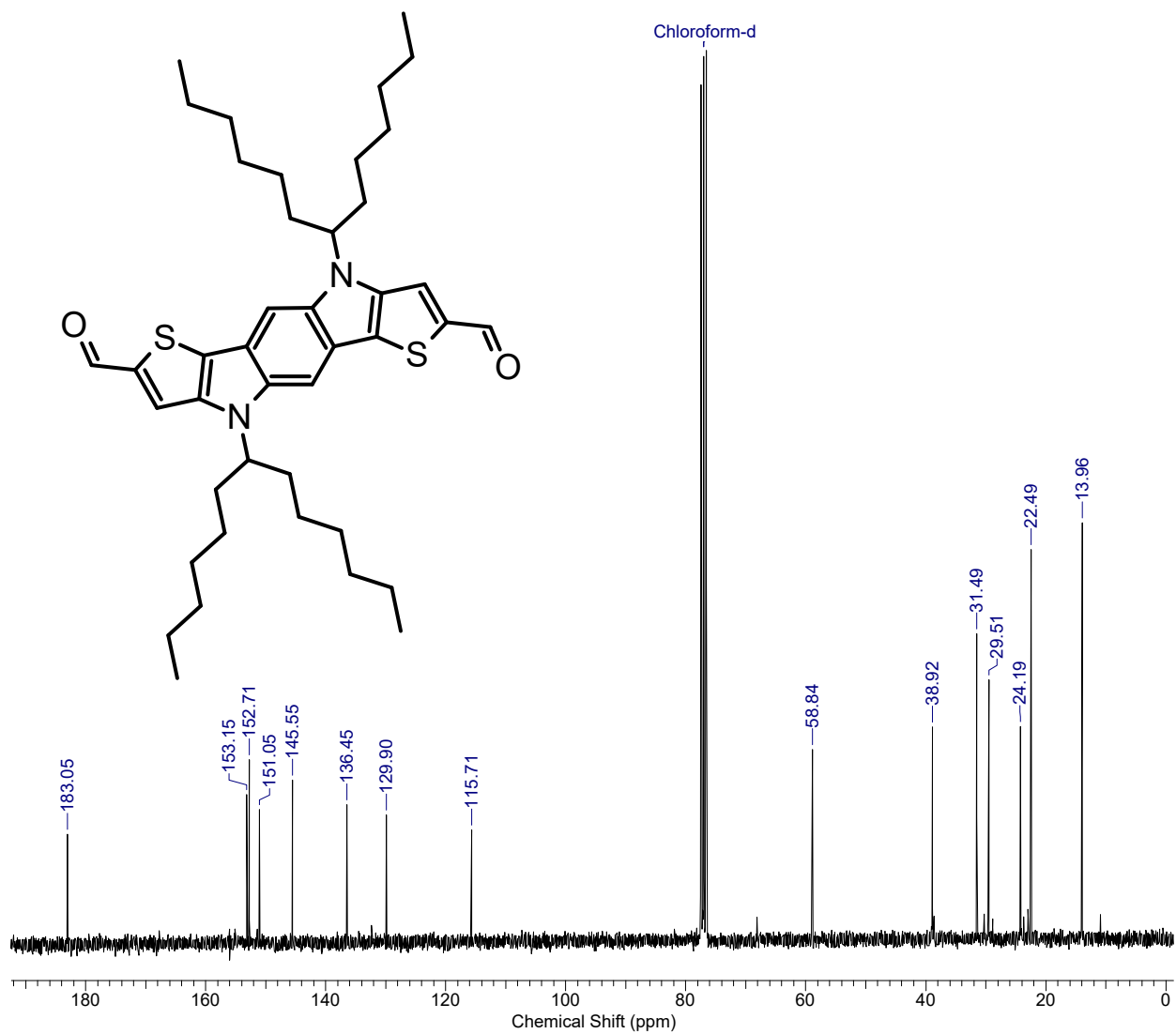
No.	(ppm)	(Hz)	Height
1	13.96	1053.8	0.4774
2	22.49	1697.3	0.4478
3	24.19	1826.1	0.2524
4	29.51	2227.5	0.3042
5	31.49	2376.8	0.3550
6	38.92	2937.4	0.2516
7	58.84	4441.2	0.2268
8	115.71	8733.2	0.1381
9	129.90	9804.6	0.1548
10	136.45	10298.9	0.1656
11	145.55	10985.6	0.1927
12	151.05	11400.8	0.1603
13	152.71	11526.3	0.2157
14	153.15	11559.4	0.1769
15	183.05	13816.3	0.1334

No.	Annotation	(ppm)
1	Chloroform-d	77.00

Fig. S6 ^{13}C NMR spectrum of compound **4** in CDCl$_3$.

No.	Annotation	(ppm)
1	Chloroform-d	7.25

No.	(ppm)	Value	Absolute Value
1	[0.78 .. 0.87]	12.022	5.33840e+7
2	[1.13 .. 1.34]	32.057	1.42354e+8
3	[1.62 .. 1.81]	8.016	3.55984e+7
4	[4.03 .. 4.20]	2.006	8.90859e+6
5	[7.45 .. 7.49]	2.012	8.93575e+6
6	[7.67 .. 7.81]	6.000	2.66421e+7
7	[7.90 .. 7.97]	2.008	8.91905e+6
8	[8.66 .. 8.77]	2.007	8.91393e+6
9	[8.88 .. 8.93]	2.003	8.89509e+6
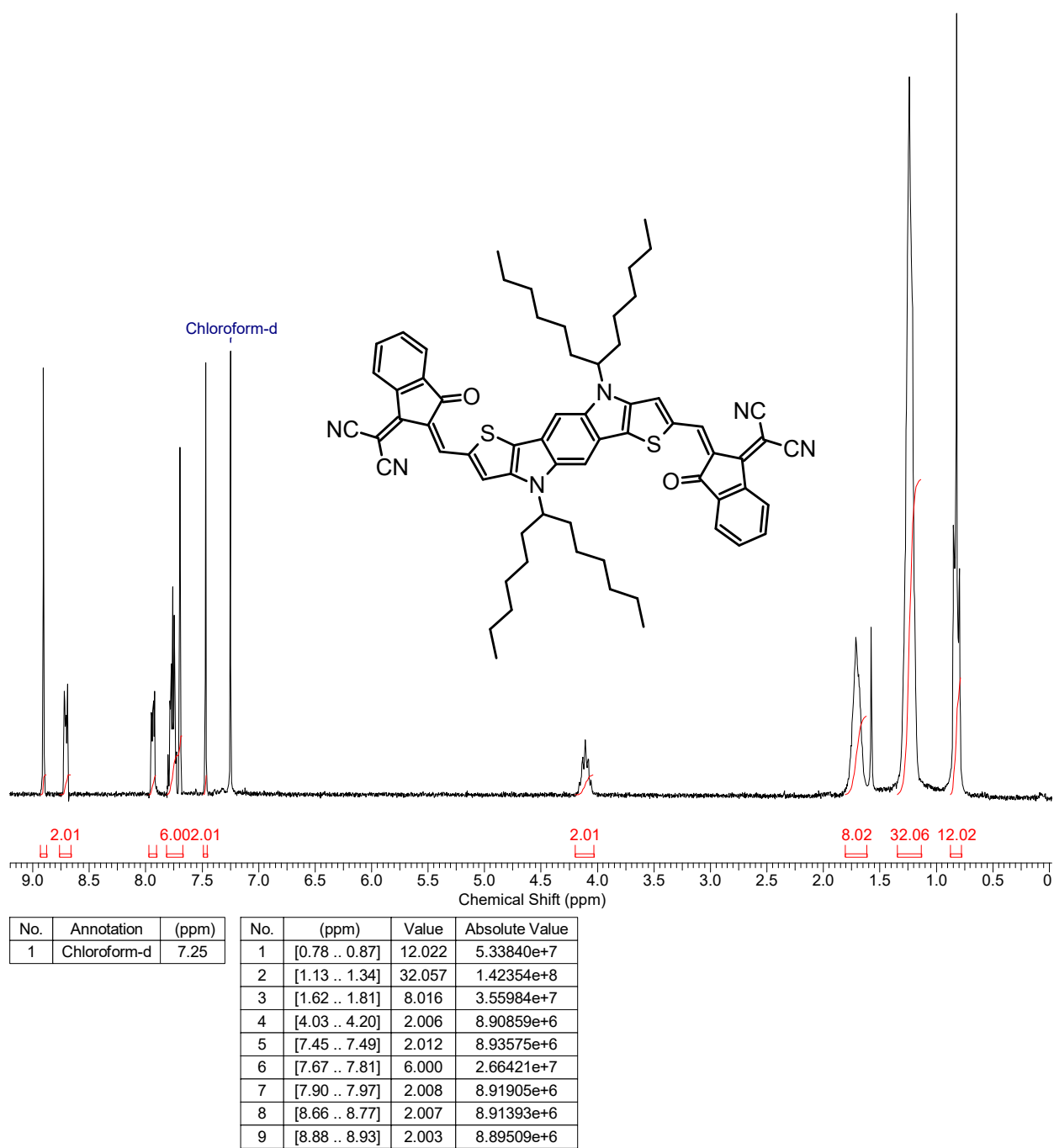
Fig. S7 ^{1}H NMR spectrum of **TPIIC** in CDCl₃.
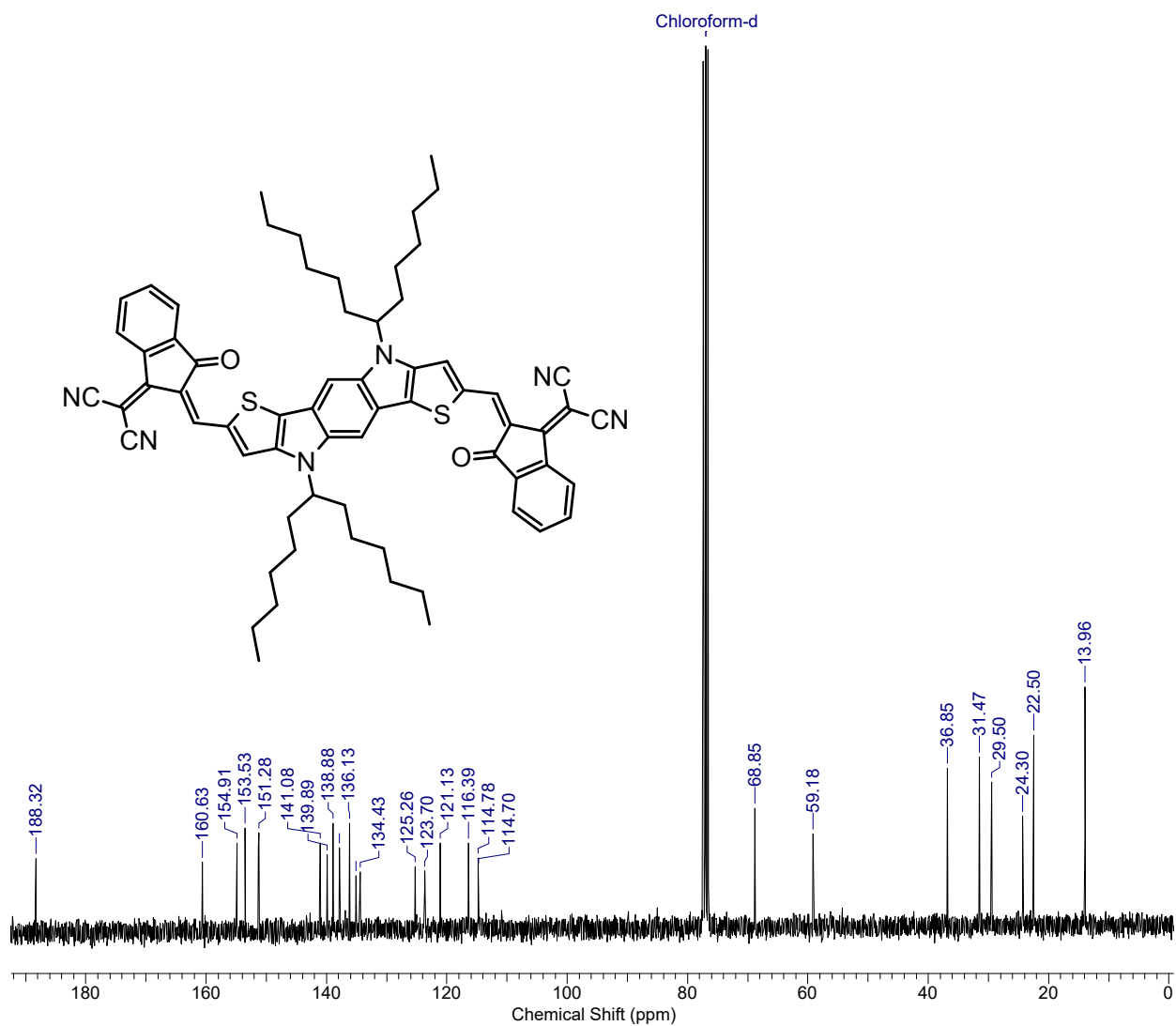
No.	(ppm)	(Hz)	Height
1	13.96	1053.8	0.2853
2	22.50	1698.4	0.2319
3	24.30	1833.9	0.1414
4	29.50	2227.0	0.1795
5	31.47	2375.1	0.2077
6	36.85	2781.5	0.1951
7	59.18	4466.7	0.1214
8	68.85	5196.4	0.1505
9	114.70	8657.4	0.0838
10	114.78	8663.5	0.0951
11	116.39	8784.6	0.1116
12	121.13	9142.8	0.1116
13	123.70	9336.3	0.0808
14	125.26	9454.7	0.0852

No.	(ppm)	(Hz)	Height
15	134.43	10146.3	0.0792
16	135.09	10196.1	0.0753
17	136.13	10275.1	0.1338
18	137.81	10401.7	0.1060
19	137.89	10407.8	0.1016
20	138.88	10482.5	0.1338
21	139.89	10558.7	0.0982
22	141.08	10648.3	0.1118
23	151.28	11418.5	0.1227
24	153.53	11588.2	0.1283
25	154.91	11692.1	0.1116
26	160.63	12123.9	0.0898
27	188.32	14213.8	0.0940

No.	Annotation	(ppm)
1	Chloroform-d	77.00

Fig. S8 ^{13}C NMR spectrum of **TPIIC** in CDCl$_3$.

2. TGA and CV and optical absorption data
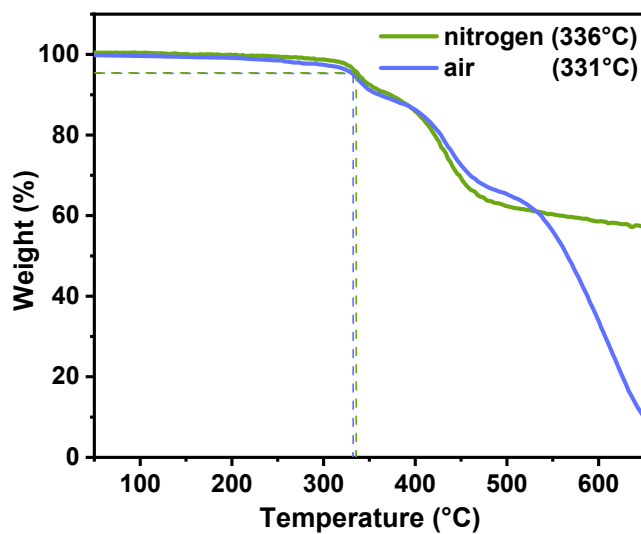
Fig. S9 Thermogravimetric analysis (TGA) curves of TPIIC.
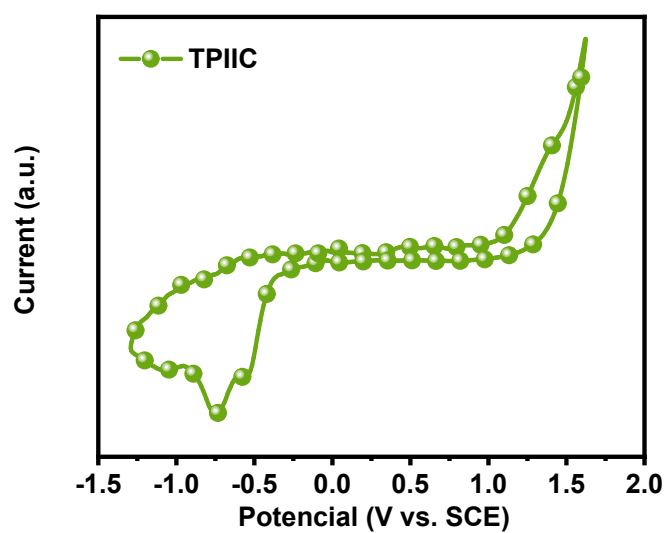
Fig. S10 Cyclic voltammetry plots of TPIIC vs SCE at the scan rate of 200 mV s^{-1}.
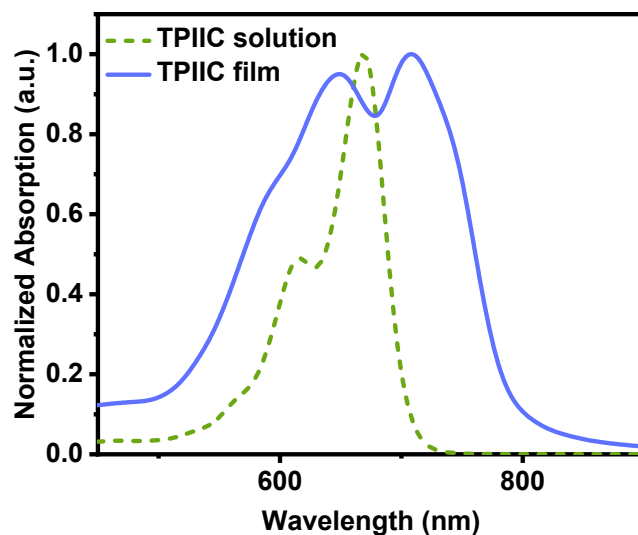
Fig. S11 *UV-vis* absorption spectra of TPIIC in chloroform solution and film cast from chloroform.

Table S1 Optical and electrochemical properties of TPIIC.

molecule	λ_{max}^{sol}(nm)	λ_{max}^{film}(nm)	φ_{ox} [a](V)	φ_{red} [a](V)	E_{HOMO} (eV)	E_{LUMO} (eV)
TPIIC	615/668	649/708	1.42	-0.48	-5.82	-3.92

[a]φ_{ox} and φ_{red} are formal oxidation and reduction potentials (vs SCE) according to CV.

3. Atomic force microscopy and Contact angle measurements .

Atomic force microscopy (AFM) measurements were performed by using a Nano Wizard 4 atomic force microscopy (JPK Inc. Germany) in Qi mode to observe the film's surface morphologies. All tests were carried out on Bruker MultiMode 8 AFM with the NanoScope V controller. Tapping mode tests parallel to the direction of stretching using Tap300Al-G silicon probes (tip radius: <10 nm; spring constant: 40 N/m; frequency: 300 kHz). Nanomechanical mapping measurements vertical to the sample stretching direction were operated at force-volume mode, using an E scanner and Multi75AL-G silicon probes. The trigger threshold of the cantilever deflection was set to 3.0 nm.
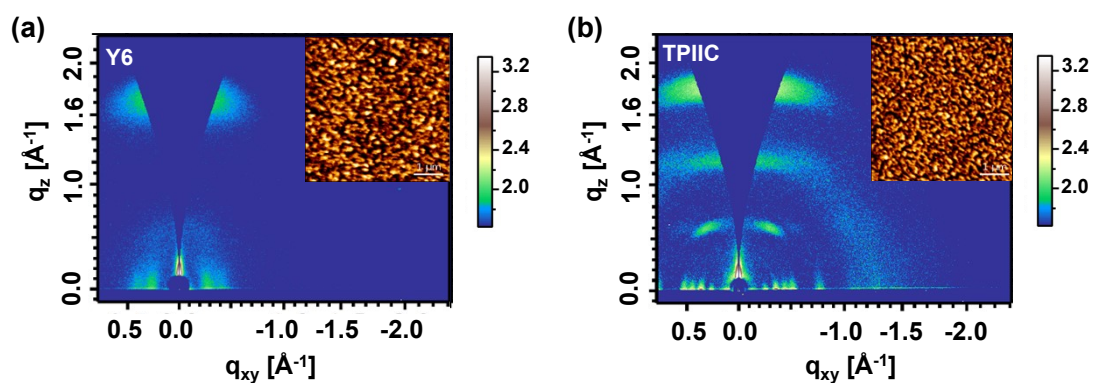
Fig. S12 2D GIWAXS pattern and corresponding AFM picture of a) Y6 and b) TPIIC.

Contact angle measurements and surface energy calculation: The contact angles of two polymer acceptors (Y6 and TPIIC) and polymer donor PM6 were measured using a Contact Angle Analyzer. The contact angles of two different solvents (water and ethylene glycol (EG)) on the neat films were used to calculate the surface tension of each film by the Wu model.[4]
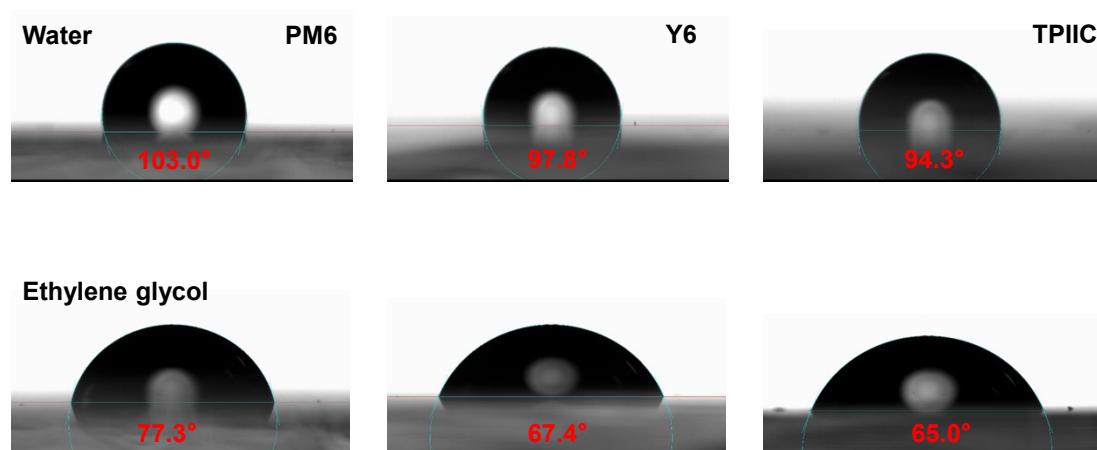

Fig. S13 Photographs of water and ethylene glycol droplets on the top surfaces of PM6, Y6 and TPIIC.

Table S2 Investigations of the contact angles, surface energy, wetting coefficient and interfacial tension values of PM6, Y6 and TPIIC.

Materials	Contact		Surface energy [mJ m^{-2}]	Relative χ	
	Water	Ethylene glycol		(With PM6)	(With Y6)
PM6	103.0 (103.0±0.05)	77.3 (77.3±0.04)	35.48 (35.48±0.06)	/	/
Y6	97.8 (97.8±0.07)	67.4 (67.44±0.06)	48.55 (48.55±0.08)	1.02 K	/
TPIIC	94.3 (94.3±0.08)	65.0 (65.0±0.05)	43.61 (43.61±0.08)	0.42 K	0.13 K

4. Device Fabrication and Testing

Control solar cell devices fabrication: The control solar cell devices were fabricated with a conventional structure of Glass/ITO/PEDOT:PSS(40 nm)/Active layer (donor: acceptor (D:A=1:1.2) for bulk heterojunction (BHJ) blend)/PNDIT-F3N(5nm)/Ag. Pre-patterned ITO coated glass substrates (purchased from South China Science & Technology Company Limited, the sheet resistance of the ITO glass was about 15 Ω washed with methylbenzene, deionized water, acetone, and isopropyl alcohol in an ultrasonic bath for 15 minutes each. After blow-drying with high-purity nitrogen, all ITO substrates are cleaned in the ultraviolet ozone cleaning system for 15 minutes. Subsequently, a thin layer of PEDOT:PSS (Xi'an Polymer Light Technology Corp 4083) was deposited through spin-coating on pre-cleaned ITO-coated glass at 4500 rpm for 20 s and dried subsequently at 150 °C for 15 minutes in atmospheric air. Then the photovoltaic layers were spin-coated in a glovebox from a solution of PM6:Y6 or PM6:Y6:TPIIC with a total concentration of 16 mg mL^{-1} in chloroform. A PNDIT-F3N layer via a solution concentration of 1 mg/mL was deposited at the top of the active layer at a rate of 4000 rpm for 30 s. Finally, the top silver electrode of 100 nm thickness was thermally evaporated through a mask onto the cathode buffer layer under a vacuum of ～5×10^{-6} mbar. The optimal active layer was fabricated by spin-coating at 3500rpm for the 30s and then thermal annealing at 100 °C for 10 mins. The thickness optimal active layer measured by a Bruker Dektak XT stylus profilometer was about 110 nm. The typical active area of the investigated devices was 5 mm^2.

The current-voltage characteristics of the solar cells were measured by a Keithley 2400 source meter unit under AM1.5G (100 mW cm^{-2}) irradiation from a solar simulator (Enlitech model SS-F5-3A). Solar simulator illumination intensity was determined at 100 mW cm^{-2} using a monocrystalline silicon reference cell with a KG5 filter. Short circuit currents under AM1.5G (100 mW cm^{-2}) conditions were estimated from the spectral response and convolution with the solar spectrum. The detail measure condition: scan voltage from -0.2 V to 1.2 V; the step is 0.02 V; the delay time is 1 ms and the scan mode is sweep. The external quantum efficiency was measured by a Solar
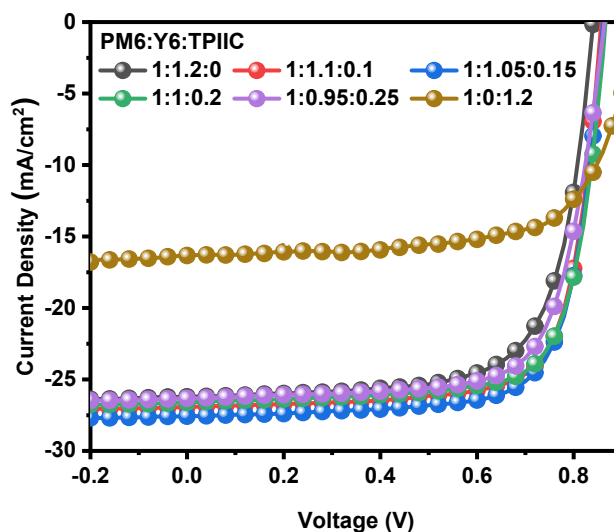
Cell Spectral Response Measurement System QE-R3011(Enli Technology Co., Ltd.).

Fig. S14 *J-V* characteristics curves of binary and ternary films with different ratios of TPIIC.

Table S3. Specific device performance of the binary and ternary devices with different TPIIC contents under the illumination of AM 1.5G (100 mW cm^{-2}).

PM6:Y6:TPIIC	V_{OC} (V)	J_{SC} (mA cm^{-2})	FF (%)	PCE[a] (%)
1:1.2:0	0.840	26.2	72.0	15.8 (15.62 ± 0.19)
1:1.1:0.1	0.857	26.9	75.2	17.4 (17.23 ± 0.16)
1:1.05:0.15	0.861	27.5	74.4	17.7 (17.55 ± 0.17)
1:1:0.2	0.866	26.6	74.7	17.2 (17.05 ± 0.14)
1:0.95:0.25	0.864	26.3	72.4	16.4 (16.23 ± 0.16)
1:0.9:0.3	0.893	24.9	69.1	15.4 (15.24 ± 0.18)
1:0:1.2	0.931	16.3	68.8	10.5 (10.37 ± 0.16)

[a]Average values with standard deviation are obtained from 10 devices.
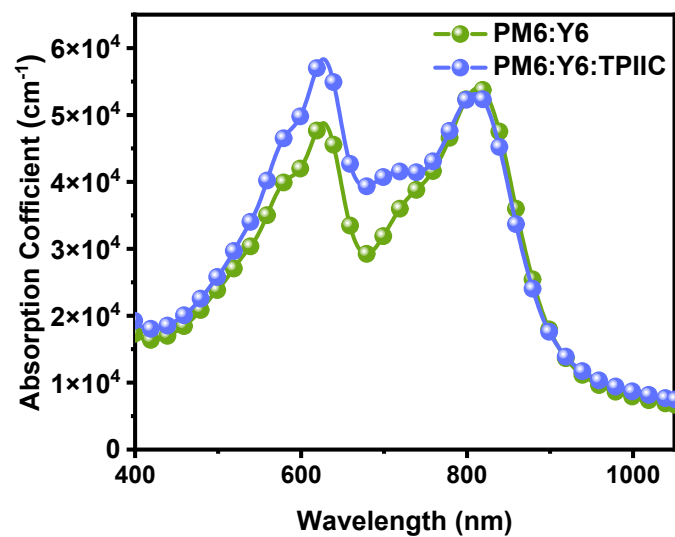
Fig. S15 *UV-vis-NIR* absorption spectra of PM6:Y6 and PM6:Y6:TPIIC films.

5. Physical measurements

Photoluminescence *measurements*: PL measurements were conducted by QE65PRO spectrometer (Ocean Optics, USA) for investigating the film formation and thermal annealing treatments. In addition, the thermal degraded PL data and emission of relevant films were collected using a Zolix Flex One Spectrometer. The PL excitation wavelength was set to 639 nm.
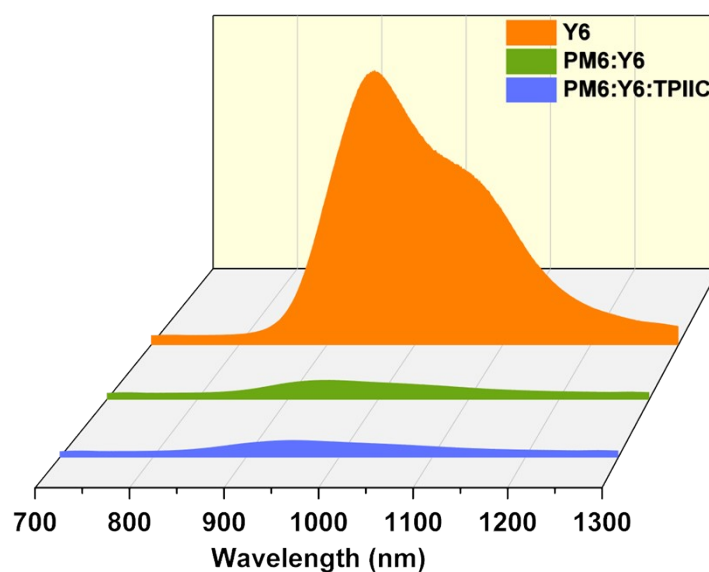

Fig. S16 The PL spectra of pristine Y6, blend PM6:Y6 and PM6:Y6:TPIIC.

Transient photocurrent (TPC) measurements: Relevant solar cells were excited with a 405 nm laser diode. The transient photocurrent response of the devices at a short circuit condition to a 200 μs square pulse from the LED with no background illumination. The current traces were recorded on a Tektronix DPO3034 digital oscilloscope by measuring the voltage drop over a 5-ohm sensor resistor in series with the solar cell. DC voltage was applied to the solar cell with an MRF544 bipolar junction transistor in a common collector amplifier configuration.

Space charge limited current (SCLC) measurements: Single carrier devices were

fabricated and the dark current-voltage characteristics were measured and analyzed in the space charge limited (SCL) regime following the reference.[5] For the electron only devices, the structure was Glass/ITO/ZnO/Active layer/PNDIT-F3N/Ag (100 nm), for the hole only devices, the structure was Glass/ITO/PEDOT:PSS/Active layer/MoO$_3$/Ag (100 nm), where the Ag was evaporated.
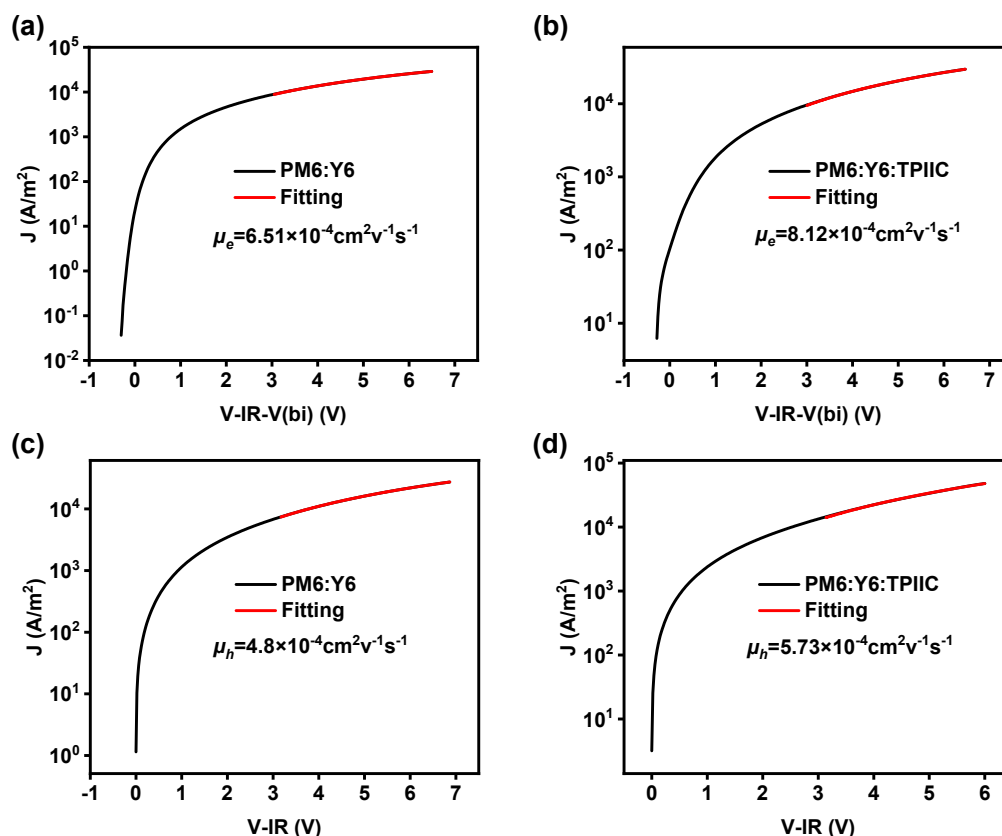

Fig. S17 a) The electron mobilities of host and b) ternary devices, the hole mobilities of c) PM6:Y6 and d) PM6:Y6:TPIIC devices measured using the SCLC approach.

Table S4 Parameters of electron mobility, hole mobility and carrier mobility of PM6:Y6 and PM6:Y6:TPIIC OSCs.

Device	μ_e ($\times 10^{-4}$ cm^2 V^{-1} s^{-1})	μ_h ($\times 10^{-4}$ cm^2 V^{-1} s^{-1})	$\mu_{carrier}$ ($\times 10^{-4}$ cm^2 V^{-1} s^{-1})	μ_e/μ_h
PM6:Y6	6.51±0.50	4.03±0.46	2.26	1.62
PM6:Y6:TPIIC	8.12±0.55	5.73±0.54	3.25	1.42

Photo-induced charge carrier extraction by linearly increasing the voltage (photo-

CELIV) measurements: In photo-CELIV measurements, the devices were illuminated with a 405 nm laser diode. Current transients were recorded across the internal 50 Ω resistor of our oscilloscope. Here, a fast electrical switch was used to isolate the device to prevent carrier extraction or sweep out. After the variable delay time, the switch connected the device to a function generator. It applied a linear extraction ramp, which was 40 μs long and 2.0 V high. Moreover, it started with an offset matching the V_{OC} of the device for each delay time. To determine the mobility in the devices, photo-CELIV curves were measured using different experimental conditions, differing in delay time and applied voltage.
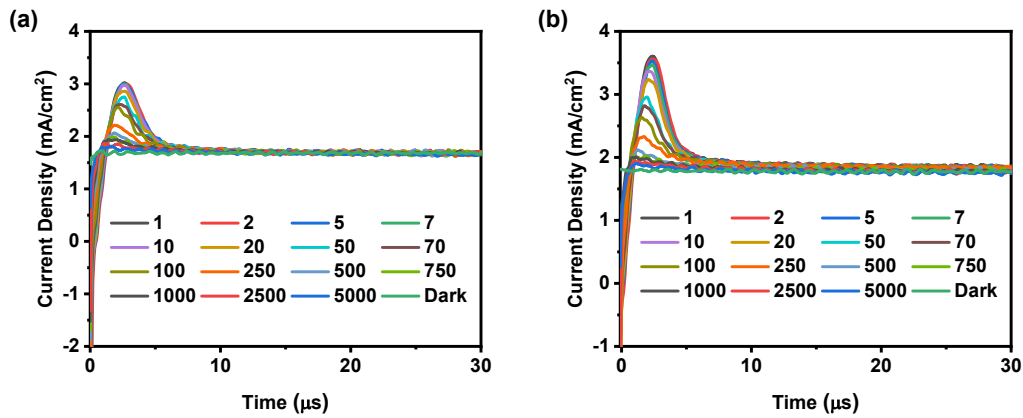
Fig. S18 Photo-CELIV measurements on the optimized a) binary and b) ternary devices for different delay times between the light pulse and the extraction voltage ramp.
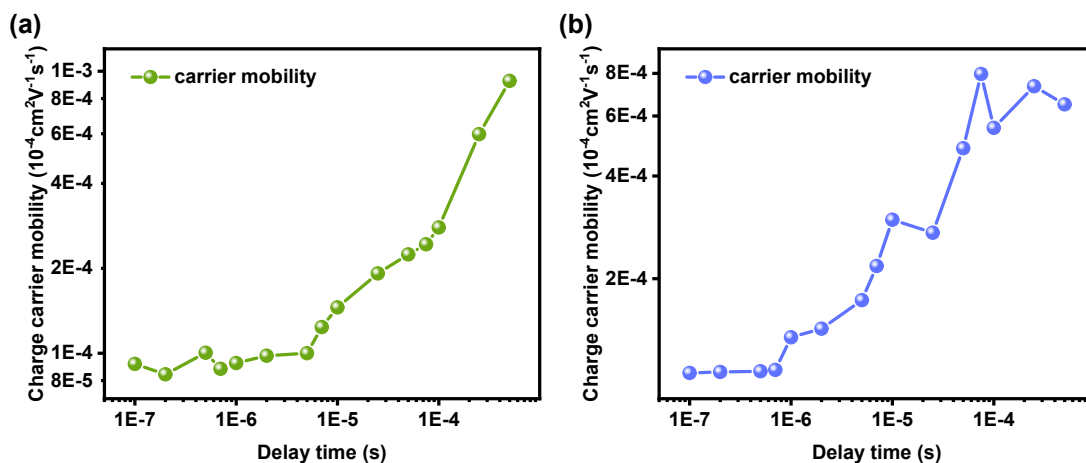

Fig. S19 Changes in carrier mobility corresponding to the delay time for a) binary and b) ternary systems obtained from photo-CELIV.

Analysis of light intensity dependent J-V characteristics: We investigated the variation of J_{SC} as a function of light intensity (decrement of change is set to 100, 90, 80, 70, 60, 50, 40, 30, 20, 10, 8, 5, calibrated with standard silicon).
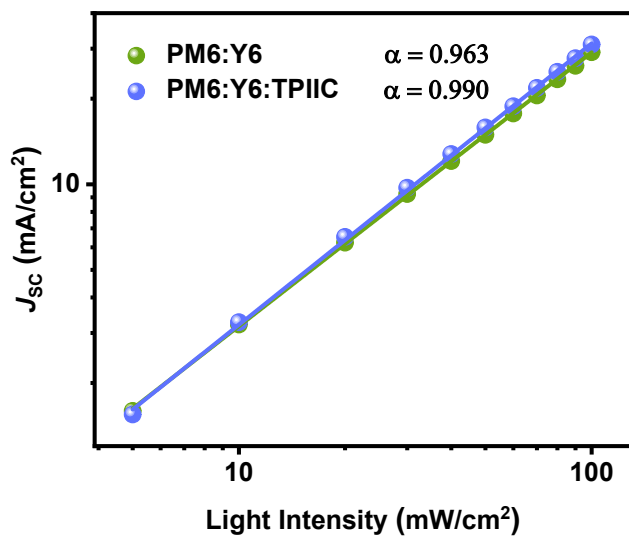

Fig. S20 J_{SC} versus light intensity of the host binary and optimal ternary devices.
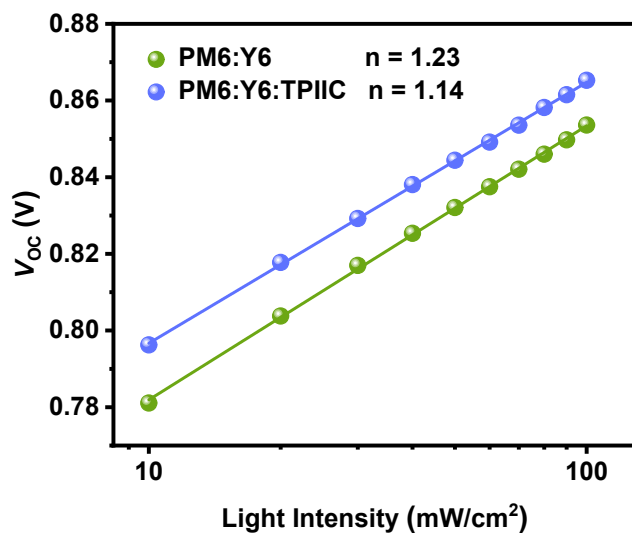

Fig. S21 V_{OC} versus light intensity of the host binary and optimal ternary devices.

Transient photovoltage (TPV) measurements: For TPV measurements, devices were directly connected to an oscilloscope in open-circuit conditions (1 MΩ). Then the device was illuminated with a white light LED at different light intensities. A small optical perturbation was applied using a 405 nm laser-diode which was adjusted in light intensity to produce a voltage perturbation of $\Delta V_O < 10\ mV \ll V_{OC}$. The amount of charges generated by the pulse was obtained by integrating a photocurrent measurement (50 Ω) without bias light.
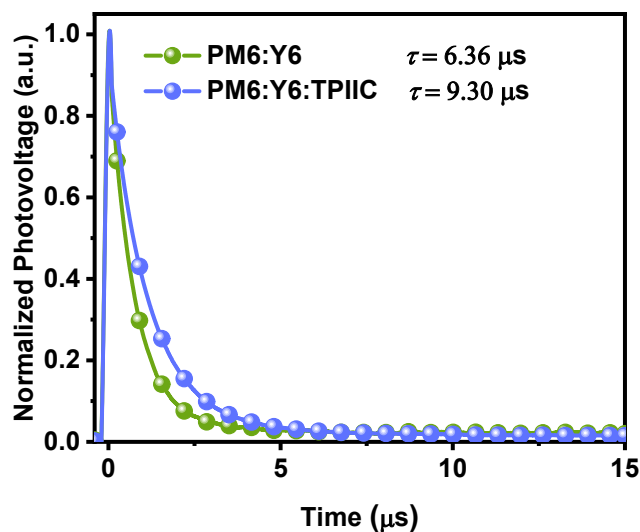

Fig. S22 Normalized transient photovoltage traces of binary and ternary devices.

6. Morphological characterizations

The grazing incidence X-ray scattering (GIWAXS) measurements were carried out with a Xeuss 2.0 SAXS/WAXS laboratory beamline using a Cu X-ray source (8.05 keV, 1.54 Å) and a Pilatus3R 300K detector. The incident angle was 0.13°. The samples for GIWAXS measurements were fabricated on silicon substrates.
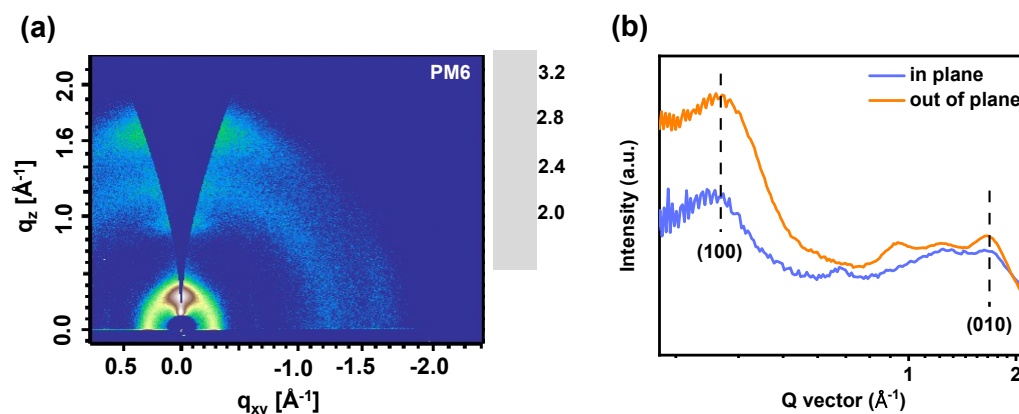

Fig. S23 2D GIWAXS patterns (a) and (b) the corresponding IP and OOP profiles of PM6 films.

Table S5 Summarized parameters for the ordering structures of PM6, Y6, TPIIC, PM6:Y6 and PM6:Y6:TPIIC from GIWAXS.

Active layers	Out-of-plane				In-plane	
	q (Å^{-1})	d-spacing (Å^{-1})	FWHM (Å^{-1})	CCL (Å)	q (Å^{-1})	d-spacing (Å^{-1})
PM6	1.6571	3.7898	0.4506	13.94	0.2984	21.046
Y6	1.7261	3.6383	0.2824	22.24		
TPIIC	1.8099	3.4698	0.1715	36.61		
PM6:Y6	1.7312	3.6275	0.3007	20.89	0.2984	21.05
PM6:Y6:TPIIC	1.7414	3.6063	0.2950	21.29	0.2984	22.05

7. Energy loss analysis

FTPS-EQE spectra measurements: The FTPS measurements were recorded using a Bruker Vertex 70 Fourier-transform infrared (FTIR) spectrometer, equipped with a quartz tungsten halogen lamp, a quartz beam-splitter, and an external detector option. A low noise current amplifier (Femto DLPCA-200) was used to amplify the photocurrent produced on the illumination of the photovoltaic devices with light modulated by the FTIR. The output voltage of the current amplifier was fed back into the external detector port of the FTIR. The photocurrent spectrum was collected by FTIR software.

Electroluminescence Measurement: The EL signature was collected with a monochromator and detected with an InGaAs detector. Data collection range is 700-1300 nm.
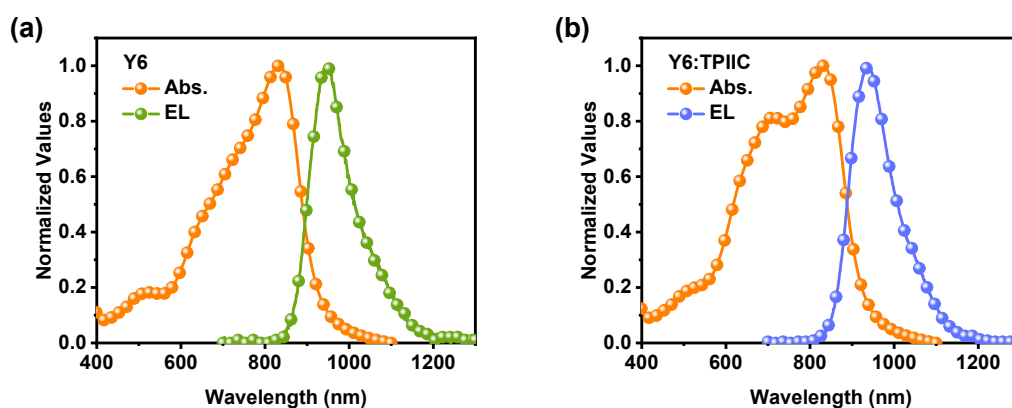

Fig. S24 Emission and absorption spectra of (a) Y6 and (b) Y6:TPIIC.

EQE-EL Measurement: Electroluminescence (EL) quantum efficiency (EQEEL) measurements were performed by applying external voltage sources through the devices from 1V to 4V. A Keithley 2400 SourceMeter was used for supplying voltages and recording injected current, and a Keithley 485 picoammeter was used for measuring the emitted light intensity.

Photoluminescence quantum yield (PLQY) measurements: The PLQY of glasses embedded with Y6, Y6:TPIIC (1:0.2, wt%), and TPIIC films was measured using a *UV-vis-NIR* quantum yield spectrometer (C13534, Quantaurus-QY Plus, Hamamatsu, Japan).

8. Stability measurements and analysis

Phototability measurements: Light-induced degradation testing: we performed light-induced degradation experiments with one sun equivalent illumination intensity for over 1000 hours on two systems investigated in this study. The solar cells were fabricated in a glovebox and aged under high vacuum, excluding the well-known effects of oxygen degradation from our experiments. To exclude any other influence of the experimental conditions on the results, all the systems were aged in the same test side by side. The investigated solar cells were built in a standard device architecture with PEDOT:PSS and PNDIT-F3N/Ag contacts.

Thermal stability testing: The testing devices were fabricated under the same preparation conditions, as mentioned above. After the evaporated of Ag, the devices were transferred to a hot plate at 85 ^oC in a N_2-filled glovebox and annealed for various time periods. All the samples for time-dependent annealing measurements were prepared under the same conditions with the thermal stability testing ones.

Differential scanning calorimetry (DSC) measurements: DSC scans were obtained with a Mettler Toledo DSC30 system with a 10 °C min^{-1} heating/cooling rate in the temperature range of 20-330 °C.
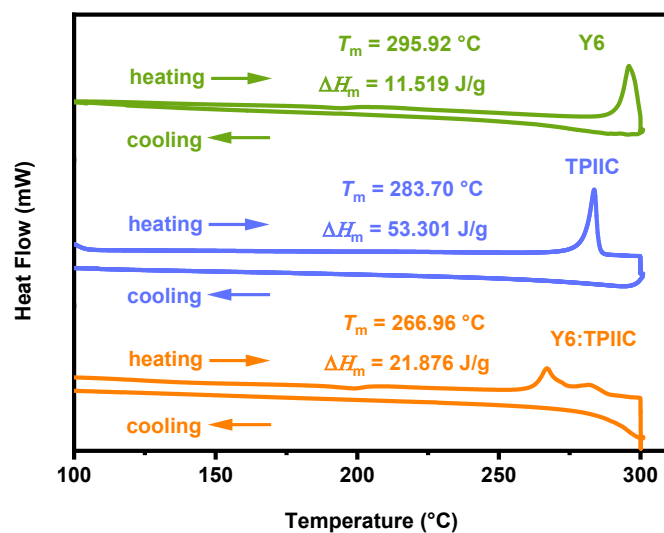

Fig. S25 The differential scanning calorimetry (DSC) curves of Y6, TPIIC and Y6:TPIIC.

Variable temperature UV–vis-NIR Measurement: All thin films subject to *UV−vis-NIR* absorption measurement were spin-cast from chloroform solutions directly onto optically transparent glass. The *UV–vis-NIR* spectra were recorded with a spectrometer after annealing individual films for 10 min. Then place it on tinfoil to cool quickly and let it cool to room temperature before testing. To minimize optical scattering induced by glass substrates, a bare glass was put into the reference optical path.
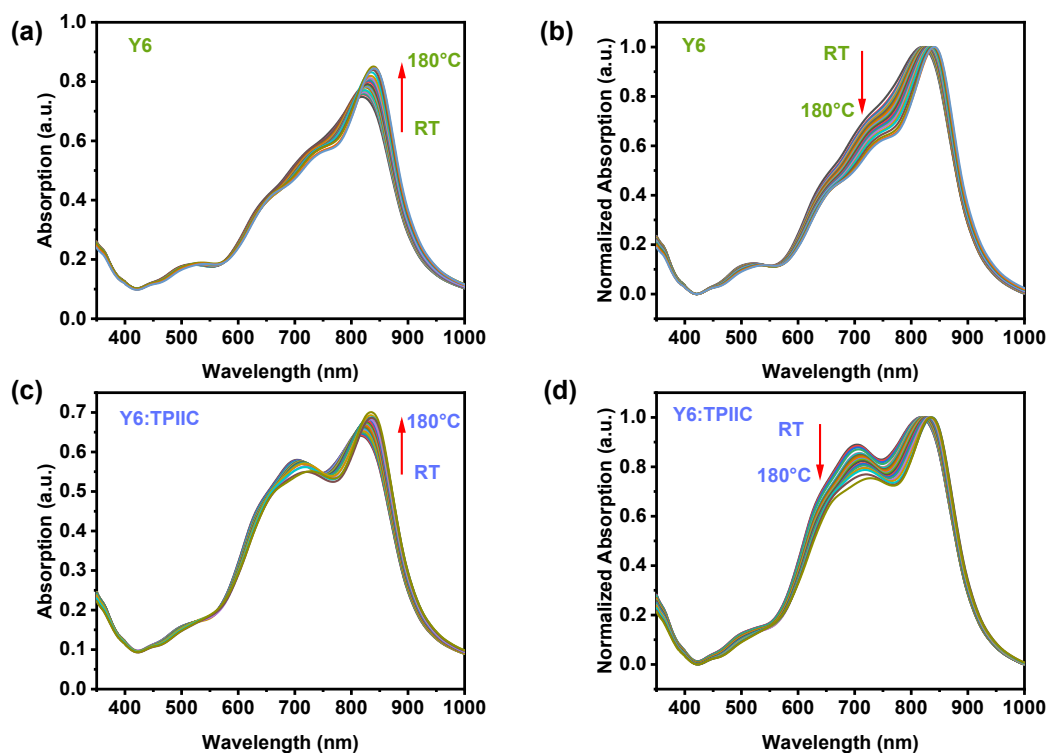

Fig. S26 *UV–vis-NIR* absorption spectra of (a) Y6 and (c) Y6:TPIIC. Normalized *UV–vis-NIR* absorption spectra of (b) Y6 and (d) Y6:TPIIC film with the increasing thermal annealing temperature.

9. References

1. J. Yuan, Y. Zhang, L. Zhou, G. Zhang, H.-L. Yip, T.-K. Lau, X. Lu, C. Zhu, H. Peng, P. A. Johnson, M. Leclerc, Y. Cao, J. Ulanski, Y. Li and Y. Zou, *Joule,* 2019, **3**, 1140-1151.

2. S. A. Ponomarenko, N. N. Rasulova, Y. N. Luponosov, N. M. Surin, M. I. Buzin, I. Leshchiner, S. M. Peregudova and A. M. Muzafarov, *Macromolecules,* 2012, **45**, 2014-2024.

3. C. M. Cardona, W. Li, A. E. Kaifer, D. Stockdale and G. C. Bazan, *Adv. Mater.,* 2011, **23**, 2367.

4. D. K. Owens and R. C. Wendt, *J. Appl. Polym. Sci.,* 1969, **13**, 1741.

5. R. Sun, J. Guo, C. Sun, T. Wang, Z. Luo, Z. Zhang, X. Jiao, W. Tang, C. Yang, Y. Li and J. Min, *Energy & Environ. Sci.,* 2019, **12**, 384-395.